

Cite this article as: Wang Zhicheng, Li Jiarong, Liu Shizhong, et al. Microstructural Characteristics of Freckles in Ni-based Single Crystal Superalloys[J]. Rare Metal Materials and Engineering, 2022, 51(10): 3533-3541.

ARTICLE

# Microstructural Characteristics of Freckles in Ni-based Single Crystal Superalloys

Wang Zhicheng, Li Jiarong, Liu Shizhong, Yang Wanpeng

Science and Technology on Advanced High Temperature Structural Materials Laboratory, Beijing Institute of Aeronautical Materials, Beijing 100095, China

**Abstract:** The as-cast microstructure, the heat-treated microstructure and the composition characteristics of freckle chains in the third generation single crystal superalloy DD9 were studied by OM, SEM, EBSD and TEM. The results show that freckles are composed of fine disorder-oriented equiaxed grains. They are in the shape of a chain roughly along the direction of crystal growth and only appear on the surface of single crystal castings. The depth and width of freckle chains are 400~800  $\mu\text{m}$ . Freckled area contains a large amount of  $\gamma/\gamma'$  eutectics. A certain amount of  $M_6C$  carbides and porosity also appear in as-cast freckled area. After heat treatment, large-size  $\gamma'$  phase and granular  $M_6C$  phase appear at the equiaxed grain boundary of freckled region. The freckled area contains more Ta and Al, but less Re and W. The composition of the freckled area is similar to the interdendritic composition.

**Key words:** single crystal superalloy; DD9; freckles; element segregation

Nickel base single crystal superalloy has become the preferred material for aeroengine turbine blade due to its excellent comprehensive mechanical properties<sup>[1-4]</sup>. In order to meet the increasing demand for thrust-to-weight ratio of aeroengine, the structure of turbine blade is becoming more and more complex, and the content of high melting point alloying elements is increasing. This brings a great challenge to the control of solidification defects in the process of turbine blade preparation<sup>[5,6]</sup>.

Stray grain, low angle boundary, sliver defects and freckles are typical grain defects in directional solidification of single crystal superalloy<sup>[7,8]</sup>. Freckles are a kind of grain defects that appear in the directional solidification process of advanced single crystal superalloy castings. It is generally believed that freckles are caused by thermal-solutal convection due to elemental segregation<sup>[9-13]</sup>. Freckles are usually in the shape of a long chain and distributed in the casting surface along the solidification direction<sup>[14]</sup>. For the essence of macro-segregation, once the freckles form on the castings, they cannot be eliminated by subsequent heat treatment, which will adversely affect the performance of the final castings<sup>[15,16]</sup>. So far, researches have shown that the formation of freckles is

influenced by the composition of the alloys<sup>[17-20]</sup>, the solidification process parameters<sup>[21,22]</sup>, the geometry of the castings<sup>[23-26]</sup> and the crystal orientation of the castings<sup>[27]</sup>.

Up to now, many researchers have studied the microstructural features of the freckle defects in single crystal castings. Giamei et al<sup>[28]</sup> found that freckle lines are linear assemblies of small random equiaxed grains which are enriched with all elements but inversely segregated ones. Chmiela's<sup>[29]</sup> investigation revealed that freckled area is characterized by high porosity and a high number of  $\gamma/\gamma'$  eutectics in PWA1426 alloy. Chen et al<sup>[30]</sup> prepared the nickel-based single crystal superalloy DD488 rods with freckle defects by reducing the temperature gradient, and found that the freckles appear in the shape of long chains which are distributed on the surface of the rod along the direction of gravity. The primary dendrite arm spacing of the freckled region is larger than that of normal region. Han et al<sup>[31]</sup> used EBSD to study the structure of the freckles in DD33 alloy and found that there are equiaxed grains with disorder-orientation in the freckled area.

Current researches on the microstructural characteristics of freckles in single crystal superalloys are focused on the as-cast

Received date: October 13, 2021

Foundation item: National Science and Technology Major Project (2017-VI-0001-0070)

Corresponding author: Li Jiarong, Ph. D., Professor, Science and Technology on Advanced High Temperature Structural Materials Laboratory, Beijing Institute of Aeronautical Materials, Beijing 100095, P. R. China, Tel: 0086-10-62497202, E-mail: jiarong.li@biam.ac.cn

Copyright © 2022, Northwest Institute for Nonferrous Metal Research. Published by Science Press. All rights reserved.

macrostructure. However, the study on the microstructural characteristics of equiaxial crystal grain in freckled area, the microstructural evolution after heat treatment, and the composition characteristic of freckled area is insufficient, especially for the single crystal superalloys with high content of refractory elements. An in-depth study on the microstructural characteristics and composition characteristics of freckles can help us to understand the formation mechanism of freckles more comprehensively and to develop effective control methods. In this study, the as-cast and heat-treated microstructures, the composition characteristics of freckles and the precipitated phase at the equiaxed grain boundary of the freckled area were studied for the third generation single crystal superalloy DD9. This study is expected to offer further understanding on the formation mechanism of freckle defects.

## 1 Experiment

The material used in this research is the third-generation single crystal superalloy DD9 developed by Beijing Institute of Aeronautical Materials. The chemical composition of DD9 alloy is shown in Table 1<sup>[32]</sup>. The master alloy was melted in a vacuum induction furnace with commercially pure raw materials. Single crystal superalloy slabs with dimensions of 200 mm×30 mm×15 mm were cast in a directional solidification vacuum furnace by conventional high rate solidification (HRS) Bridgman technique. Seed crystal method was employed to obtain single crystal specimens. To obtain freckles, a relatively low withdrawal rate was applied in the directional solidification. The heat treatment regime of DD9 alloy is as follows: pre-heat treatment+1340 °C/6 h/air cooling+1140 °C/4 h/air cooling+870 °C/32 h/air cooling.

The microstructures of freckled and normal areas were observed by optical microscope (OM) and FEI Nova450 field emission scanning electron microscope (FE-SEM). The composition of freckled and normal area was tested by X-Max-50 energy dispersive spectroscopy (EDS). Electron back scattered diffraction (EBSD) was used to analyze the size and orientation distribution of equiaxed grains in freckled area. The primary dendrite arm spacing and the content of eutectics were counted by metallographic analysis software Image-pro

Plus 6.0. The specimens for OM and FE-SEM observation were polished and etched with a chemical etchant of 100 mL H<sub>2</sub>O+80 mL HCl+25 g CuSO<sub>4</sub>+5 mL H<sub>2</sub>SO<sub>4</sub> for 5~10 s. Specimens for EBSD test were electropolished. The electrolyte was 80% anhydrous methanol+20% sulfuric acid, and the electrolysis was conducted at 20~30 V for 10~15 s. TEM samples were prepared by focused ion beam (FIB).

## 2 Results and Discussion

### 2.1 Microstructure of freckles

Fig. 1 shows the macro-etched morphology of freckles in single crystal superalloy slabs. It can be seen that the freckles only appear on the surface and edges of the castings. They exist in the shape of chains, roughly along the solidification direction. Fig. 2 shows the metallographic microstructures of freckled and normal areas in single crystal superalloy DD9. Fig. 2a is the transverse section microstructure and Fig. 2b is the longitudinal section microstructure of as-cast freckles. As can be seen, misoriented dendritic fragments appear in the freckled area, and a large amount of eutectics are present around the dendritic fragments. It is worth pointing out that freckles only appear on the surface of the castings. Statistics reveal that the depth and the width of freckles are 400~800 μm on the surface of the castings. Fig. 2c shows the as-cast transverse section microstructure of the normal area. Compared with the normal area, the freckled area contains more eutectics. Tertiary dendrites can be observed near the freckled area as shown in Fig. 2a. Fig. 3 shows the average primary dendrite arm spacing and the content of eutectics in freckled and normal areas. The average primary dendrite arm spacing in freckled area is 487 μm which is much larger than 347 μm in normal area. The average secondary dendrite arm spacing in normal area is 88 μm. The heat-treated microstructure of freckles is shown in Fig. 2d. A large amount of eutectics can be found in the freckled area after heat treatment, which suggests that heat treatment process cannot eliminate freckle defects.

The microstructural characteristics of the freckles were further studied by EBSD and the results are shown in Fig. 4. The EBSD analysis provides a detailed description for the crystallographic orientation of freckled area. The orientation

Table 1 Chemical composition of single crystal superalloy DD9 (wt%)

Cr	Co	Mo	W	Re	Al	Ta	Nb	Hf	C	Y	Ni
3.5	7	2	6.5	4.5	5.6	7.5	0.5	0.1	0.008	0.001	Bal.

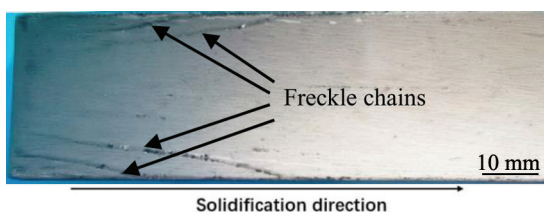


Fig.1 Macro-etched morphology of the freckle chains in single crystal superalloy slabs

map and inverse pole figure (IPF) in Fig. 4b and 4c show the orientation of equiaxed grains in the freckled area. Freckle grains have a quite different orientation and deviate from the matrix orientation. The grain size distribution and the misorientation angle distribution of the equiaxed grains are shown in Fig. 5a and 5b, respectively. The average grain size is 151 μm. It can be seen that the orientation of equiaxed grains in the freckled area is disordered and 70% of orientation deviation between grains and matrix is less than 10°. This

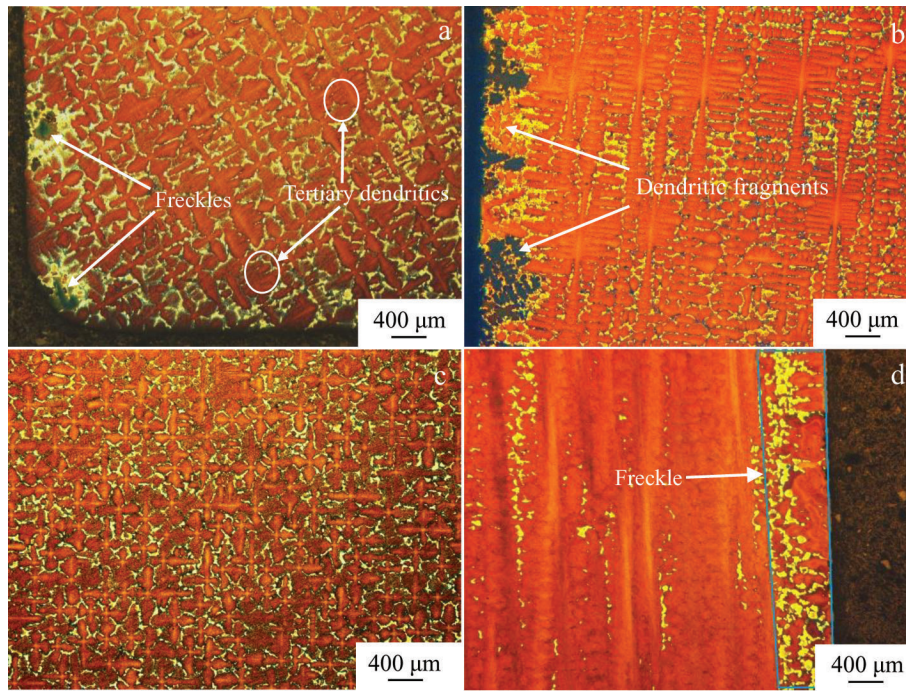


Fig.2 OM microstructures of freckled and normal areas in DD9 alloy: (a) as-cast transverse section microstructure of freckles; (b) as-cast longitudinal section microstructure of freckles; (c) as-cast transverse section microstructure of normal area; (d) heat-treated longitudinal section microstructure of freckles

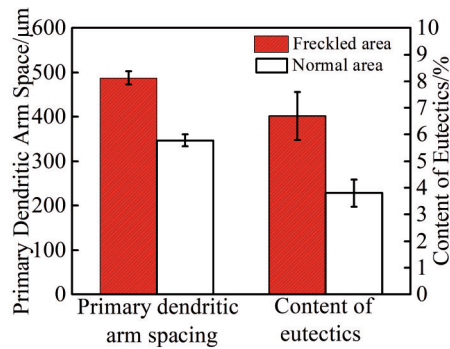


Fig.3 Comparison of primary dendritic arm spacing and eutectics content in freckled and normal areas

suggests that freckle chains are composed of fine equiaxial grains with disorder orientation.

Fig. 6 shows the as-cast and heat-treated longitudinal section microstructures of freckled area. Compared with normal area, more solidification porosity can be seen in freckled area and most porosity appears near the  $\gamma/\gamma'$  eutectics which can be seen from Fig.6a. Fig.6b shows the heat-treated microstructure of freckles. After heat treatment, large amounts of  $\gamma/\gamma'$  eutectics and porosity still exist in the grain boundary in freckled area, which suggests that heat treatment cannot eliminate  $\gamma/\gamma'$  eutectics in freckled area.

Further studies were conducted on the boundary of equiaxed grains of the as-cast freckled area. Fig. 7a reveals that massive blocky precipitated phases appear in the grain boundary which are near the eutectics. The morphology of the blocky precipitated phase cut by FIB is shown in Fig. 7b. Fig.7c shows the results of composition analysis of the blocky precipitated phase, and it discloses that precipitated phase is

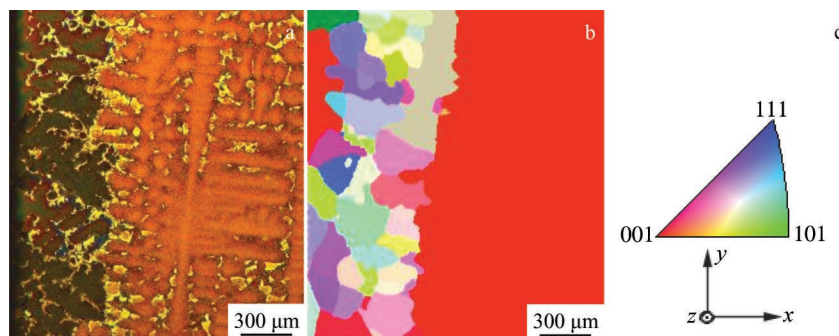


Fig.4 Microstructural characteristics of as-cast freckles: (a) longitudinal section microstructure of as-cast freckles, (b) orientation map of freckled area, and (c) corresponding IPF

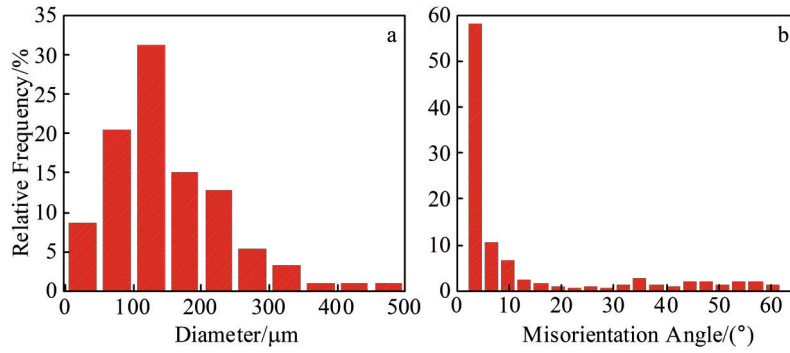


Fig.5 Grain size distribution (a) and misorientation angle distribution (b) of equiaxed grains in freckled area

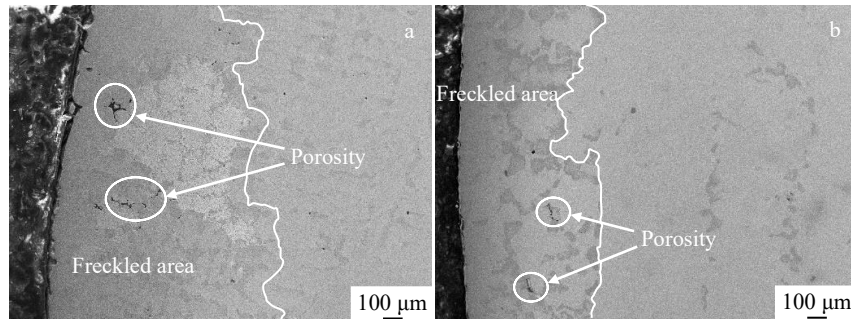


Fig.6 Solidification porosity in freckled area: (a) as-cast and (b) heat-treated

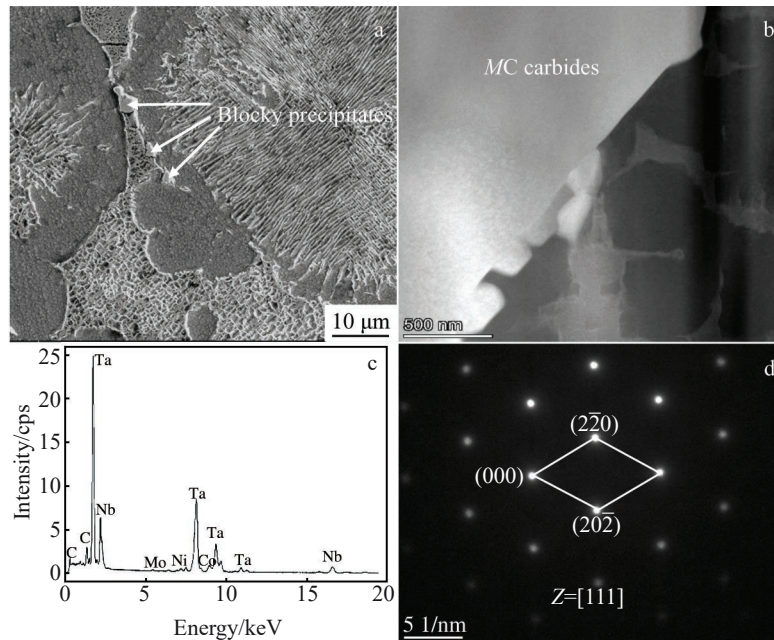


Fig.7 Precipitated phase at grain boundary of as-cast freckled equiaxed grains: (a) location of precipitated phase in freckled area; (b) morphology of precipitated phase obtained by FIB; (c) EDS spectrum of precipitated phase; (d) SAED pattern of precipitated phase

rich in element Ta. Combined with SAED result in Fig.7d, it can be determined that the blocky precipitated phase is Ta-rich  $MC$  type carbides. Further research on the distribution of elements in the blocky precipitated phase and matrix is shown in Fig. 8. Another kind of banded precipitates rich in Re, W, Mo can be seen at the edge of the block  $MC$  type carbide.

Composition analysis of the banded precipitated phase is shown in Fig.9a. Combined with SAED result in Fig.9b, it can be assured that the banded precipitated phase is Re-, W-, Mo-Ta-rich  $M_6C$  type carbides.

Fig. 10a shows the microstructure of the freckled area after heat treatment, which indicates that freckled area still contains

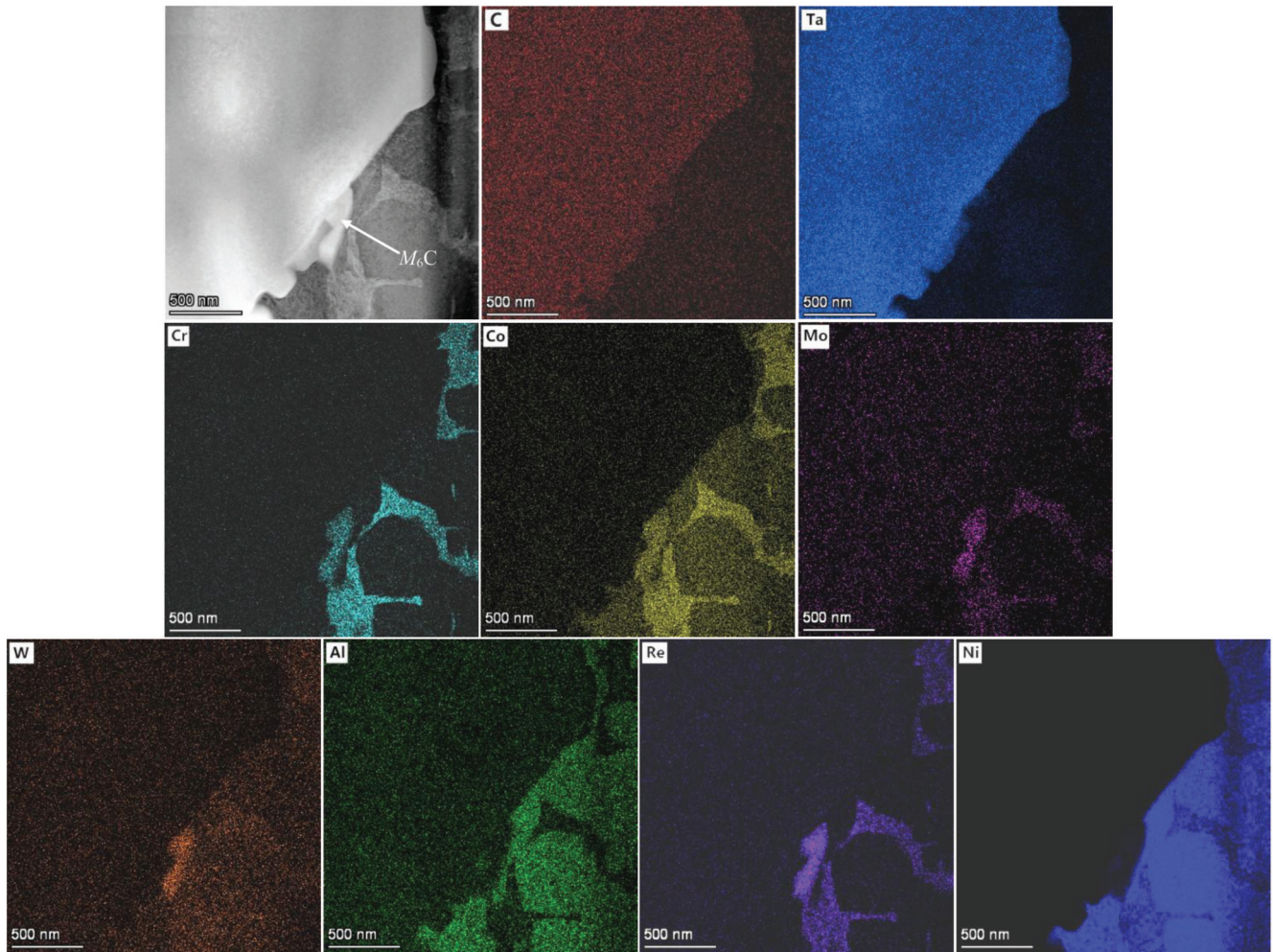


Fig.8 Morphology and distribution of elements in precipitated phase and matrix

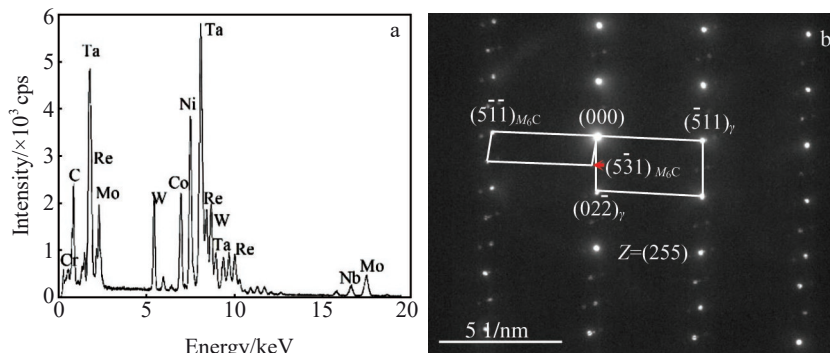


Fig.9 EDS spectrum (a) and SAED pattern (b) of the banded precipitated phase near the  $M_6C$  carbides at grain boundary of as-cast freckled equiaxed grains

a large amount of  $\gamma/\gamma'$  eutectics after heat treatment. As shown in Fig.10b, after heat treatment, grain boundary with a width of about 4  $\mu\text{m}$  appears among equiaxed grains in the freckled region, and coarse  $\gamma'$  phase and a large number of granular precipitates are precipitated at the grain boundary. TEM samples were prepared by FIB, and the composition and the crystal structure of granular precipitates at grain boundary were analyzed. The result is shown in Fig.10c and 10d. It

suggests that the precipitates are  $M_6C$  type carbides rich in W, Re, Mo and Ta, which is similar to the  $M_6C$  type carbides in as-cast freckled area shown in Fig.9a.

### 2.2 Component characteristics of freckle defects

Table 2 makes a comparison among the composition of freckled area, dendrite core and inter-dendritic of normal area. The results show that there are more Ta and Al in the freckled area, but less Re and W in the freckled area, whose

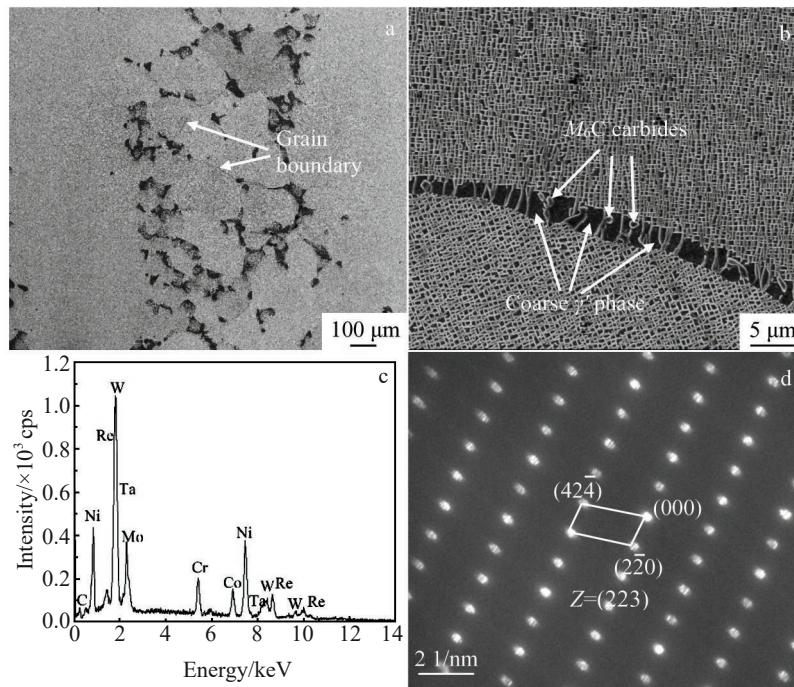


Fig.10 Analysis of microstructure and precipitated phase at equiaxed grain boundary of freckled area after heat treatment: (a) equiaxed grain in freckled area after heat treatment; (b) equiaxed grain boundary and precipitated phase at grain boundary; (c) EDS spectrum of precipitated phase at grain boundary; (d) SAED pattern of precipitated phase

**Table 2** Composition comparison among as-cast dendrite core, inter-dendritic of normal area and freckled area (wt%)

Element	W	Re	Al	Ta	Cr	Co	Mo	Ni
Dendritic core	9.3	6.9	4.9	3.9	3.2	7.1	1.2	Bal.
Inter-dendritic	4.8	3.0	6.1	7.1	3.2	6.3	1.4	Bal.
Freckled area	5.6	3.2	6.4	6.1	3.4	6.4	1.5	Bal.

composition is more similar to the inter-dendritic regions. The element partition coefficients of the freckled and normal area are statistically analyzed, which are shown in Fig.11 (element segregation coefficient  $k_i = C_g/C_j$ , where  $C_g$  is the content of element in dendrite core and  $C_j$  is the content of element in inter-dendritic region). It can be seen that for the element segregated into the dendrite core such as Re, W, Co, their segregation coefficient  $k_i$  in freckled area is greater than

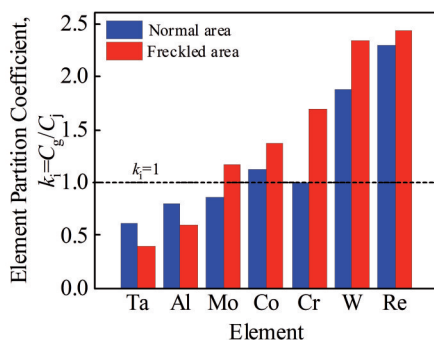


Fig.11 Element segregation coefficient between dendritic core and interdendritic region in normal and freckled area

that in the normal area. In contrast, for the element segregated into the interdendritic region such as Al and Ta, their segregation coefficient  $k_i$  in freckled area is less than that in the normal area. It suggests that the element segregation in the freckled area is more serious.

### 3 Discussion

Up to now, it has been generally agreed that freckles initiate due to the formation of dendritic fragments which are caused by thermosolutal convection in the mushy zone<sup>[33,34]</sup>. The thermo-solutal convection is driven by a density inversion originating from inter-dendritic segregation. During upward directional solidification of single crystal superalloy, light alloy elements (with a partition coefficient less than unity, like Al, Ta) are preferentially rejected into the melt. At the same time, heavy alloy elements (with a partition coefficient greater than unity, like Re, W) are preferentially incorporated into the solid. Such micro-segregation can cause the local melt density to decrease and result in the gravitationally instability of the melt inside the mushy zone. When the degree of density inversion reaches a certain level, convection will occur in the liquid phase.

The application of the microscale numerical model proposed by Kao<sup>[35]</sup> has demonstrated that the distribution and size of freckles are strongly dependent on the transverse thermal profile. The conventional Bridgman directional solidification furnace used in this experiment has a certain lateral temperature gradient, which makes the solidification interface concave<sup>[36]</sup>. Philippe's research shows that due to the existence of the lateral temperature gradient, the liquid phase

in the mushy zone is subjected to horizontal force<sup>[37]</sup>. Philippe deduced the formulas for the calculation of horizontal (perpendicular to the primary dendritic) permeability and vertical (parallel to the primary dendritic) permeability of the liquid phase in the mushy zone during the directional solidification of single crystal superalloys as follows<sup>[37]</sup>:

$$k_x = 3.62 \times 10^{-3} f_l^{3.34} \lambda_1^{0.699} \lambda_2^{2.73} \quad (1)$$

$$k_y = 3.75 \times 10^{-4} f_l^2 \lambda_1^2 \quad (2)$$

where  $k_x$  is permeability in the horizontal direction,  $m^2$ ;  $k_y$  is permeability in the longitudinal direction,  $m^2$ ;  $\lambda_1$  is primary dendrite arm spacing,  $m$ ;  $\lambda_2$  is secondary dendrite arm spacing,  $m$ ;  $f_l$  is liquid fraction.

Researches show that liquid phase in the mushy zone has the greatest convection tendency,  $f_l=0.5$  in directional solidification of single crystal superalloys<sup>[38]</sup>, so the value of  $f_l$  is chosen to be 0.5 in this study. Take the values of  $\lambda_1=347 \mu m$  and  $\lambda_2=88 \mu m$  into Eq.(1) and Eq.(2), and obtain  $k_x=6.37 \times 10^{-11} m^2$  and  $k_y=1.49 \times 10^{-11} m^2$ .

Permeability characterizes the resistance of liquid convection. The greater the permeability, the smaller the resistance. Thus it can be deduced that fluid flow along horizontal direction is noticeably easier than that along longitudinal direction because the former permeability is about 4 times greater than that of the latter, so it is reasonable to think that the existence of lateral temperature gradient will promote the lateral liquid convection.

Based on the above analysis, the formation mechanism of freckles on the specimen is proposed. Fig. 12 shows the schematic diagram of freckles formation. There is not only vertical convection but also horizontal convection of the segregated liquid in the mushy zone. Partial dendrite fragments caused by liquid convection in the mushy zone reach the edge of the sample with the liquid flow. At the same time, the heat dissipates more quickly at the edge of the sample than in the inside, so the cooling rate is larger at the edge of the sample. Due to vertical convection along the edges of the sample, dendrite fragments will solidify and form freckles along the direction of gravity along the edges. In addition, another part of the dendritic fragments are solidified in the convection channel before reaching the edge of the sample, resulting in the formation of inclined freckle chains,

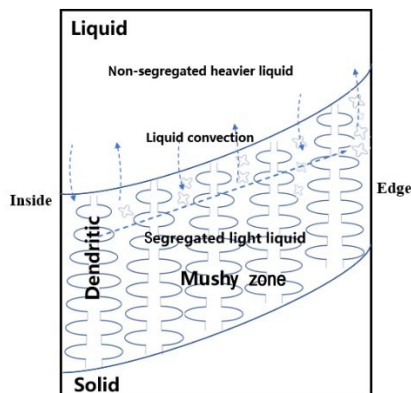


Fig.12 Schematic diagram of freckles formation

as shown in Fig. 1. Due to the disorder orientation of these dendrite fragments, equiaxed grains with disorderly orientation will form in freckled area after solidification. Recently, Reinharta et al<sup>[39]</sup> have observed the directional solidification process of CMSX-4 alloy through synchrotron radiation X-rays and found that the dendrite fragments with disorder orientation appear on the edge of the sample, which agrees with the results of this study. As a result of the narrow liquid convection channel, the affected zone is at the scale of the primary dendritic arm. Therefore, the depth and width of the freckled region are observed to be 400~800  $\mu m$ , which is comparable to the average dendritic spacing of the freckled region of 487  $\mu m$ .

Al and Ta produce positive segregation to inter-dendritic region during directional solidification of single crystal superalloy, while Re, W produce negative segregation to dendritic core<sup>[40]</sup>. Table 2 shows that compared with normal area, the freckled area contains more Al, Ta and less Re, W, indicating that the composition of the freckled area is more similar to the composition of inter-dendritic region. Compared with the normal area, the composition of dendrite core in the freckled area is similar to that of the normal area, but the inter-dendritic region contains more Al and Ta, and less Re and W in the freckled area. Therefore, as shown in Fig. 11, the element segregation in the freckled area is greater, making the segregation coefficient of elements Al and Ta smaller, while the segregation coefficient of Re and W elements is larger.

The presence of a large amount of Al and Ta in the freckled area leads to the formation of plenty of  $\gamma/\gamma'$  eutectics, as shown in Fig. 3. At the same time, the higher Ta content in the liquid phase also leads to the formation of Ta-rich  $M_6C$  carbides, as shown in Fig.7a. Due to the formation of coarse fan-shaped  $\gamma/\gamma'$  eutectics in the freckled area, the final solidification position of the freckled area is not well fed, and much solidification porosity appears in the freckled area, as shown in Fig.6a.

After heat treatment, coarse  $\gamma'$  phase and granular  $M_6C$  carbides are precipitated on the equiaxed grains boundary in freckled area, as shown in Fig. 10b. These granular  $M_6C$  carbides are different from the banded  $M_6C$  carbides in as-cast microstructure. Coarse  $\gamma'$  phase and granular  $M_6C$  carbides are mainly formed by the reaction of blocky  $M_6C$  carbides and  $\gamma$  phase during the heat treatment. This reaction can be clarified by Eq.(3), which is consistent with the evolution mechanism of carbides in single crystal superalloy studied by Liu et al<sup>[41]</sup>:



## 4 Conclusions

1) Freckles only appear on the surface of the single crystal superalloy castings, and a large number of dendritic fragments appear in the freckled area. Freckles are composed of fine disorder-orientated equiaxed grains. Compared with normal area, more  $\gamma/\gamma'$  eutectics form in the freckled area, and the dendrite arm spacing is larger in as-cast freckled area.

2) A certain amount of solidified micro-porosity and a few Ta-riched  $M_6C$  carbides appear around the fan-shaped eutectics

in the as-cast freckled area. After heat treatment, grain boundary of the equiaxed grains in freckled area becomes wider, and coarse  $\gamma'$  phase and  $M_6C$  phase rich in Ta, Re, Mo and W precipitate at the grain boundary.

3) Compared with the normal area, the freckled area contains more Ta and Al but less Re and W. The element segregation in the freckled area is more serious. The composition of the freckled region is more similar to that of the interdendritic region.

## References

- Cetel A D, Duhal D N. *Superalloys 1988*[C]. Warrendale: Seven Springs, 1988: 235
- Harris K, Erickson G L, Sikkenga S L. *Superalloys 1992*[C]. Warrendale: Seven Springs, 1992: 297
- Walston W S, Ohara K S, Ross E W et al. *Superalloys 1996*[C]. Warrendale: Seven Springs, 1996: 27
- Li Jiarong, Zhong Zhenggang, Tang Dingzhong et al. *Superalloys 2000*[C]. Warrendale: Seven Springs, 2000: 777
- Zhang Jun, Huang Taiwen, Liu Lin et al. *Acta Metallurgica Sinica*[J], 2015, 51(10): 1163 (in Chinese)
- Pollock T M, Tin S. *Journal of Propulsion and Power*[J], 2006, 22(2): 361
- Zhao Jinqian, Li Jiarong, Liu Shizhong et al. *Rare Metal Materials and Engineering*[J], 2007, 36(12): 2232 (in Chinese)
- Zhou Yizhou, Green N R. *Superalloys 2008*[C]. Warrendale: Seven Springs, 2008: 317
- Frueh C, Poirier D R, Felicelli S D. *Materials Science and Engineering A*[J], 2002, 328(1-2): 245
- Felicelli S D, Heinrich J C, Poirier D R. *Journal of Crystal Growth*[J], 1998, 191(4): 879
- Beckermann C, Gu J P, Boettinger W J. *Metallurgical and Materials Transactions A*[J], 2000, 31(10): 2545
- Auburtin P, Wang T, Cockcroft S L et al. *Metallurgical and Materials Transactions B*[J], 2000, 31(4): 801
- Saad A, Gandin C A, Bellet M et al. *Metallurgical and Materials Transactions A*[J], 2015, 46(11): 4886
- Copley S M, Giamei A F, Johnson S M et al. *Metallurgical and Materials Transactions B*[J], 1970, 1(8): 2193
- Li Qiudong, Shen Jun, Qin Ling et al. *Materials Characterization*[J], 2017, 130: 139
- Reed R C, Tao T, Warnken N. *Acta Materialia*[J], 2009, 57(19): 5898
- Pollock T M, Murphy W H, Goldman E H et al. *Superalloys 1992*[C]. Warrendale: Seven Springs, 1992: 125
- Pollock T M, Murphy W H. *Metallurgical and Materials Transactions A*[J], 1996, 27(4): 1081
- Tin S, Pollock T M, King W T. *Superalloys 2000*[C]. Warrendale: Seven Springs, 2000: 201
- Tin S, Pollock T M. *Metallurgical and Materials Transactions A* [J], 2003, 34(9): 1953
- Schadt R, Wagner I, Preuhs J. *Superalloys 2000*[C]. Warrendale: Seven Springs, 2000: 211
- Ma Dexin, Zhou bin, Polaczek A B. *Advanced Materials Research*[J], 2011, 278: 428
- Ma Dexin, Wu Q, Polaczek A B. *Metallurgical and Materials Transactions B*[J], 2012, 43(2): 344
- Ma Dexin, Polaczek A B. *Metallurgical and Materials Transactions A*[J], 2014, 45(3): 1435
- Hong Jianping, Ma Dexin, Wang Jun et al. *Journal of Alloys and Compounds*[J], 2015, 648: 1076
- Ma Dexin. *Acta Metallurgica Sinica*[J], 2016, 52(4): 426 (in Chinese)
- Ma D X, Mathes M, Zhou B. *Advanced Materials Research*[J], 2011, 278: 114
- Giamei A F, Kear B H. *Metallurgical and Materials Transactions B*[J], 1970, 1(8): 2185
- Chmiel A B, Sozansk A M, Cwajna J S. *Archives of Materllurgy and Materials*[J], 2012, 57(2): 559
- Chen Jingyang, Wu Wenjin, Li Qing et al. *The Chinese Journal of Nonferrous Metals*[J], 2018, 28(12): 2494 (in Chinese)
- Han Dongyu, Jiang Weiguo, Xiao Juhan et al. *Journal of Alloys and Compounds*[J], 2019, 805: 218
- Li Jiarong, Liu Shizhong, Wang Xiaoguang et al. *Superalloys 2016*[C]. Warrendale: Seven Springs, 2016: 57
- Yuan L, Lee P D. *Acta Materialia*[J], 2012, 60(12): 4917
- Karagadde S, Yuan L, Shevchenko N et al. *Acta Materialia*[J], 2014, 79: 168
- Kao A, Shevchenko N, Alexandrakis M et al. *Philosophical Transaction A*[J], 2019, 377: 1
- Elliott A J, Pollock T M. *Metallurgical and Materials Transactions A*[J], 2007, 38(4): 871
- Philippe B. *Thesis for Doctorate*[D]. Columbia: University of British Columbia, 1998, 16
- Madison J, Spowart J, Rowenhorst D et al. *Acta Materialia*[J], 2010, 58(8): 2864
- Reinharta G, Grangeb D, Abou K L et al. *Acta Materialia*[J], 2020, 194: 68
- Seo S M, Lee J H, Yoo Y S et al. *Superalloys 2008*[C]. Warrendale: Seven Springs, 2008: 277
- Liu Lirong, Jin Tao, Sun Xiaofeng et al. *Journal of Aeronautical Materials*[J], 2007, 27(5): 12 (in Chinese)

## 镍基单晶高温合金雀斑组织特征

王志成, 李嘉荣, 刘世忠, 杨万鹏

(北京航空材料研究院 先进高温结构材料重点实验室, 北京 100095)

**摘要:** 采用OM、SEM、EBSD、TEM等方法研究了第3代单晶高温合金DD9雀斑铸态、热处理态组织及化学成分特征。结果表明: 雀斑是由取向杂乱、细小的等轴晶粒组成, 通常平行于晶体生长方向, 呈链状分布在铸件的表面, 其深度与宽度为400~800  $\mu\text{m}$ ; 雀斑区域含有大量 $\gamma/\gamma'$ 共晶, 且出现一定量的 $MC$ 、 $M_6C$ 型碳化物和疏松。热处理后雀斑区域等轴晶粒边界出现大尺寸 $\gamma'$ 相及颗粒状的 $M_6C$ 相。雀斑区域含有较多Ta、Al等元素, 而Re、W等元素含量较少, 雀斑区域成分更加接近枝晶间成分。

**关键词:** 单晶高温合金; DD9; 雀斑; 元素偏析

---

作者简介: 王志成, 男, 1993年生, 博士, 北京航空材料研究院先进高温结构材料重点实验室, 北京 100095, 电话: 010-62497202, E-mail: zhicheng0356@163.com